

HOW DO WE PROSPECT FOR ICE AT THE MOON'S SOUTH POLE? R. C. Elphic¹, D. J. Lawrence¹, V. R. Eke², L. F. A. Teodoro³, G. J. Taylor⁴, D. B. J. Bussey⁵, ¹Space Science and Applications Group, Mail Stop D466, Los Alamos National Laboratory, Los Alamos, NM 87545 USA (relphic@lanl.gov). ²Department of Physics, University of Durham, Durham DH1 3LE, UK, ³Astronomy and Astrophysics Group, Department of Physics and Astronomy, University of Glasgow, Glasgow G12 8QQ, UK, ⁴Hawai'i Institute of Geophysics & Planetology, University of Hawaii, Manoa, HI 96822 USA, ⁵Johns Hopkins Applied Physics Laboratory, Laurel, MD 20723 USA.

Introduction: Locations of permanent shadow at the lunar poles are potential sites for significant concentrations of cold-trapped volatiles, including water ice [1,2]. Besides being of immense scientific value, such concentrations may also enable *in situ* resource utilization. While Lunar Prospector results indicate enhanced hydrogen at the poles [3,4,5], considerable controversy exists concerning whether orbital and Earth-based radar data indicate the presence of ice [6] or rocks and rough topography at small scales [7]. Even if ice is present only interstitially in regolith, it can have high concentrations. *Thus, a top priority of future lunar exploration must be to thoroughly assess the physical state, distribution, abundance and stratigraphy of volatile-bearing deposits.* We use a new Pixon-based image reconstruction algorithm together with a map of permanent shadow to effectively improve spatial resolution of Lunar Prospector neutron measurements [8]. We find that hydrogen abundances vary widely between cold traps. If the hydrogen/ice distribution within a shadowed crater such as Shackleton is also inhomogeneous at kilometer scales and less, then much higher abundances are plausible in scattered locations within the crater. But this constitutes a challenge to mission planning and execution.

South Pole Shadow Model: Clementine imagery and radar observations indicate that sizeable areas of the Moon's poles are permanently shadowed. In small, simple craters (<20 km diameter) alone, there is an estimated 7500 and 6500 km² in permanent shadow for the north and south poles, respectively [9]. We combine that model of simple craters with the south pole radar digital elevation model [10], and calculate the illumination given by the lunar spin axis tilt of 1.5° during south polar summer. Finally, illumination derived from Clementine imagery is used to exclude any spuriously shadowed pixels. As might be expected, the floors of Shackleton, Shoemaker, de Gerlache, Faustini and other craters are in permanent shadow. We obtain a total shadowed area of ~12,150 km² for the south polar region.

Pixon Deconvolution Procedure: The ~45 km size of the Lunar Prospector neutron spectrometer footprint prevents us from determining plausible ice abundances in polar craters directly. We attempt to improve the spatial resolution by deconvolving the

epithermal flux map using a variant of the Pixon image restoration technique [8]. This approach sharpens and restores imagery only where it is statistically permissible to do so. The code searches for the least complicated (lowest information content) map that is consistent with the data, the statistical uncertainties and the instrument point-spread function.

We apply a further very powerful constraint to the pixon deconvolution process: locations that are occasionally in sunlight are only permitted to have at most solar wind abundances (≤ 166 ppm H, or 0.15 wt% WEH). Locations in permanent shadow are allowed to have between 0 and 20 wt% WEH. The latter limit is consistent with pore-filled ice in the regolith.

Figure 1, panel A shows the recovered Pixon epithermal count rate map for the region within approximately 5 degrees of the south pole. Panel B shows the corresponding WEH abundance for the same region.

Ice Prospecting in Shackleton: The inferred WEH abundance in south polar permanently shadowed cold traps is inhomogeneous – values range from less than 0.1 to over 1 wt%. This inhomogeneity may well extend to smaller scales within craters as well. In Shackleton we see on average an epithermal count rate of 16 counts/sec, consistent with ~0.4 wt% WEH. But a linear combination of drier and wetter parcels is also consistent. Panel C shows this trade-off as a color contour plot of the fractional area of 'wet' parcels on the crater floor: the abscissa is $\log_{10}(\text{WEH}_2)$, the assumed water-equivalent hydrogen abundance in 'wet' parcels, while the ordinate is WEH_1 , the water-equivalent hydrogen abundance of 'dry' parcels. The color code denotes the 'wet' area fraction.

The 'dry' regolith in cold permanent shadow may preferentially retain higher concentrations of solar wind hydrogen than at lower latitudes, owing to lower diffusion rates. Suppose this cold regolith contains 0.25 wt% WEH from solar wind implantation (about five times the average amount in returned soils and regolith breccias). Then panel C tells us that the 'wet' parcels of ~1 wt% WEH would occupy a large fractional area of 0.5; but if 'wet' parcels contain ~20 wt% WEH, they would occupy only 0.1 fractional area of the crater floor.

What this means for "water ice" detection from a landed lunar polar mission is shown in panel D. Here

we see the number of sites that must be sampled to ensure a 90% probability of detection of “wet” parcels with WEH_2 , given surrounding “dry” parcels with WEH_1 . If the “wet” and “dry” parcels have 1 wt% and 0.25 wt% WEH respectively, then only 4 or so sites are required. But if “wet” parcels are ice-rich, with 20 wt% WEH , then their more areally limited extent means more than 15 sites must be visited to be 90% certain of detection. Thus, thorough sampling over a wide region is necessary to characterize the distribution of WEH , especially since we do not know the characteristic scale size of plausible deposits. It would be much more straightforward to establish scale size, areal fraction, abundance and burial depth of icy deposits using a neutron spectrometer on a rover sam-

pling a broad range of scales, rather than with a hit-or-miss hopper approach.

References: [1] Watson, K., Murray, B. C. & Brown, H., (1961) *J. Geophys. Res.* **66**, 3033-3045. [2] Arnold, J. R. (1979) *J. Geophys. Res.* **84**, 5659-5668. [3] Feldman W. C. et al. (1998) *Science*, **281**, 1496–1500. [4] Feldman W. C. et al. (2001) *JGR-Planets*, **106**, 23,231-23,251. [5] Lawrence, D. J. et al. (2006) *JGR-Planets*, **111**,10.1029/2005JE002637. [6] Nozette S. et al. (1996) *Science*, **274**, 1495-1498. [7] Campbell, D. B. et al. (2006) *Nature* **443**, 835-837. [8] Eke, V. (2001) *Mon. Not. R. Astron. Soc.* **324** (1), 108-118 [9] Bussey, D. B. J. et al. (2003) *GRL*, **30**, doi:10.1029/2002GL016180. [10] Margot, J-L. et al (1999) *Science* **284**, 1658-1660.

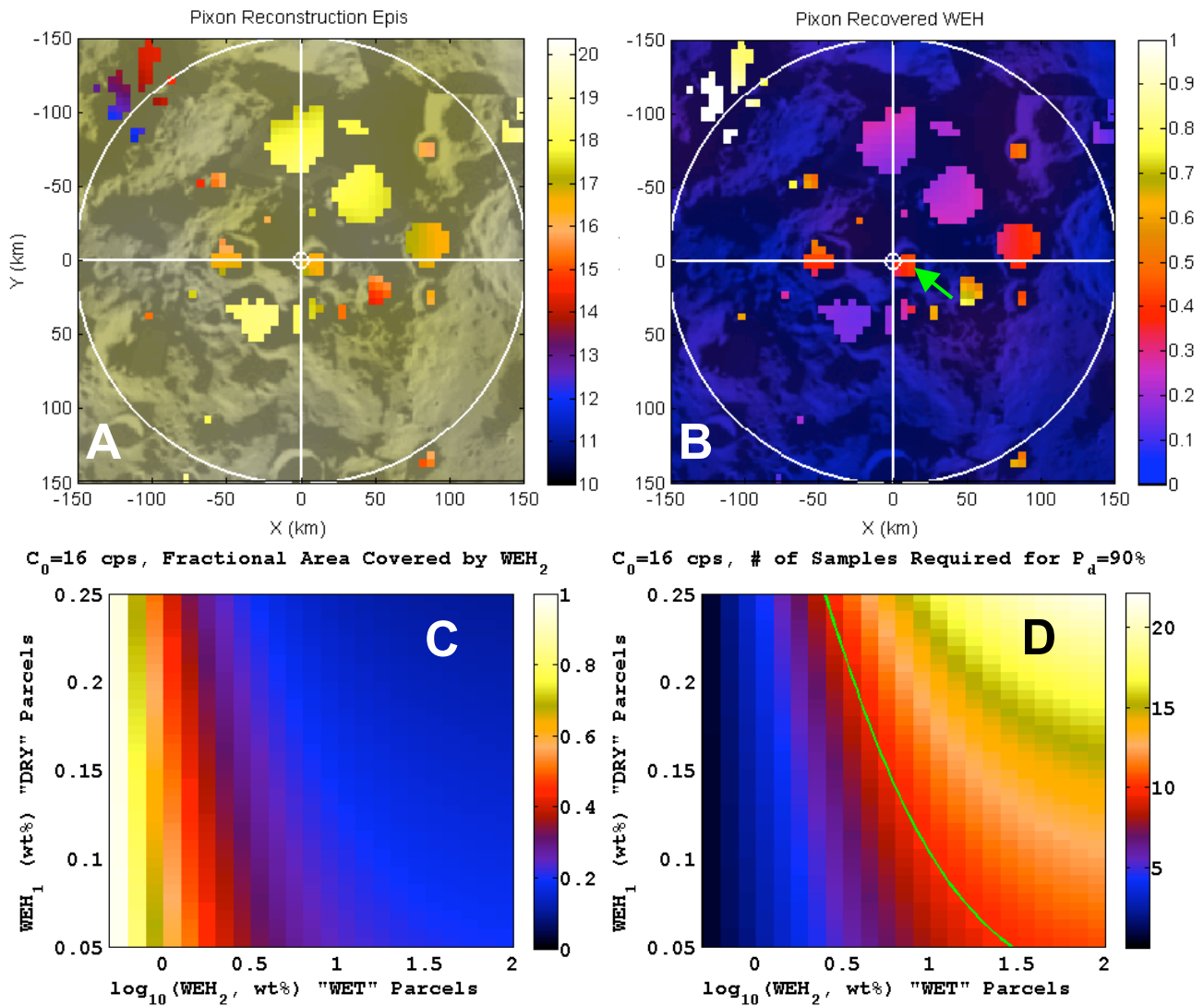


Figure 1. (A) Recovered, deconvolved epithermal count rate map. (B) WEH in wt% from Panel A. Green arrow points to Shackleton crater. (C) Fractional crater floor area covered by “wet” parcels of water-equivalent hydrogen abundance WEH_2 given “dry” parcel WEH_1 . (D) Number of randomly-selected sites needed to provide 90% probability of detection for WEH_2 given “dry” parcel WEH_1 . Green line denotes 10-site contour.